catalysts

MDPI

Article

Enhanced Soot Oxidation Activity of a CuO-Doped CeO_2 Catalyst via Acid Etching

Changlong Zheng [1], Xiaodong Wu [1,*], Zhenguo Li [2], Rui Ran [3] and Duan Weng [1]

[1] Key Laboratory of Advanced Materials of Ministry of Education, School of Materials Science and Engineering, Tsinghua University, Beijing 100084, China; zhengcl2023@tsinghua.edu.cn (C.Z.); duanweng@tsinghua.edu.cn (D.W.)
[2] National Engineering Laboratory for Mobile Source Emission Control Technology, China Automotive Technology & Research Center, Tianjin 300300, China; lizhenguo@catarc.ac.cn
[3] State Key Laboratory of New Ceramics and Fine Processing, School of Materials Science and Engineering, Tsinghua University, Beijing 100084, China; ranr@tsinghua.edu.cn
* Correspondence: wuxiaodong@tsinghua.edu.cn; Tel.: +86-010-62-792-375

Abstract: Copper oxides tend to agglomerate on the surface of CeO_2, with a high amount of Cu. In this study, a CeO_2 catalyst with a high CuO doping amount was treated with nitric acid to improve its catalytic performance for soot oxidation. The effect of acid etching on the structural properties of the CuO-doped CeO_2 catalyst were elucidated. The characterization results indicated that aggregated CuO particles formed over CuCe. The acid etching resulted in a remarkable increase in the surface area of CuCe. Additionally, acid etching promoted the formation of surface-adsorbed oxygen species and oxygen vacancy, and reduced the content of CuO_x species with weak interaction with CeO_2. The soot temperature-programmed oxidation results show the acid etching of CuCe catalyst could reduce the T_{50} from 443 to 383 °C. The isothermal reaction results also suggest that acid etching of CuCe leads to an increase in reaction rate from 16.2 to 46.0 μmol min^{-1} g^{-1}.

Keywords: CeO_2; Cu species; acid etching; surface oxygen; bulk oxygen vacancies; soot oxidation

Citation: Zheng, C.; Wu, X.; Li, Z.; Ran, R.; Weng, D. Enhanced Soot Oxidation Activity of a CuO-Doped CeO_2 Catalyst via Acid Etching. *Catalysts* **2023**, *13*, 1463. https://doi.org/10.3390/catal13121463

Academic Editor: Paul McGinn

Received: 26 October 2023
Revised: 18 November 2023
Accepted: 21 November 2023
Published: 23 November 2023

1. Introduction

The soot particles emitted by diesel engines can trigger respiratory and cardiovascular diseases, leading to severe health problems [1,2]. The most common after-processing technology for hindering soot discharge is the use of diesel particulate filters (DPFs) to trap particulates. The diesel exhaust temperature (200–500 °C) cannot meet the ignition temperature of soot (>600 °C) [3]. Hence, oxidation catalysts must be applied for catalyzing soot oxidation at lower temperatures. In the past decades, a good diversity of catalysts such as precious metal catalysts [4], CeO_2-based oxides [5], and transition metal oxides [6] have been applied to soot removal for achieving DPFs regeneration. Because of the scarcity of precious metals, there is always an increasing impetus to exploit cost-effective and active alternatives to noble metal catalysts. In comparison with noble metals, inexpensive CeO_2 and transition metal oxides are promising catalysts for soot combustion [7,8].

It was reported that modification of transition metal oxides via wet chemistry or impregnation methods is an efficient way of improving the redox ability of CeO_2 catalysts [9]. Replacing Ce^{4+} with Fe^{x+}, Co^{x+}, and Mn^{x+} can promote the formation of oxygen vacancies, thereby accelerating the diffusion of surface and bulk oxygen species and achieving improved soot oxidation activities [8,10]. Among transition metals, Cu mainly exists in three valence states of Cu^0, Cu^+ and Cu^{2+}, which can promote the reduction/oxidation process of ceria via the Mars–van Krevelen (Mv-K) mechanism [11,12]. Liang et al. [13] suggested that Cu can improve the oxidation reaction by activating the O_2 molecules on the surface and regulating the oxygen spillover to the ceria support. Due to the unique catalytic performance of Cu, it has gained tremendous attention from researchers. For example, the

binary CuO-CeO_2 system has been widely investigated in many catalytic reactions, such as soot oxidation [14], CO oxidation [15], and volatile organic compound oxidation [16].

Liang et al. [13] prepared CuO-doped CeO_2 catalysts for soot oxidation using the sol-gel method. The results showed that CuO_x nanoclusters highly dispersed on the surface of CeO_2 are responsible for the activation of lattice oxygen, resulting in the enhancement of the soot oxidation activity of CuO-CeO_2 (T_m = 356 and 522 °C in 10% O_2 under tight and loose contact conditions). Wang et al. [17] suggested that highly dispersed copper species favor the enhanced redox capability of three-dimensionally ordered macroporous CuO–CeO_2 catalysts at low temperatures, thus resulting in an enhanced soot oxidation (T_m = 551 and 427 °C in 5.0% O_2 and 2500 ppm NO/5.0% O_2 under loose contact conditions). Andana et al. [18] found that CuO/CeO_2 catalysts are active for soot oxidation at low temperatures under an NO atmosphere due to the early NO evolution (T_{50} = 552 and 534 °C in 10% O_2 and 550 ppm NO/10% O_2 under loose contact conditions). Piumetti et al. [19] fabricated a set of $Ce_{1-x}Cu_xO_2$ (*x* ranging from 0.05 to 0.95) oxide catalysts, and evaluated the soot oxidation activity. The results showed that the $Ce_{0.95}Cu_{0.05}O_2$ binary oxide catalyst exhibits the best catalytic activity (T_m = 384 °C in 50% air/50% N_2 under tight contact conditions). Cui et al. [20] synthesized CuO-doped CeO_2 nanosheets and evaluated their soot oxidation performance. The results demonstrated that CuO doping promoted the formation of oxygen species on the surface of CeO_2, and enhanced the soot oxidation activity (T_{50} = 312 °C in 5% O_2 under tight contact conditions; T_{50} = 360 °C in 1000 ppm/5% O_2 under loose contact conditions). However, excessive CuO doping would suppress the catalytic activity of CeO_2. Acid etching of catalytic materials can improve structural properties, thus influencing catalytic activity. For example, Zhao et al. [21] synthesized high-surface-area perovskite oxides $LaMnO_{3+\delta}$ via an acid-etching method, and favorable NO catalytic oxidation activity was observed on the etched catalysts. Liang et al. [22] also found that nitric acid etching of Ag@CeO_2 significantly increased the defect sites of CeO_2 and improved the electrocatalytic performance.

In this study, a CuO-doped CeO_2 catalyst was prepared via a hydrothermal method, and was then subjected to an acid-etching process. The intrinsic reactivity of the catalysts for soot oxidation was evaluated via temperature programmed oxidation (TPO) and an isothermal reaction model under tight contact conditions. The results showed that acid etching significantly improved the soot oxidation activity of the CuCe catalyst, and the corresponding mechanism of acid etching was discussed.

2. Results and Discussion

2.1. Catalytic Activities for Soot Oxidation

The intrinsic activities of the catalysts were evaluated by conducting a soot–TPO reaction under tight contact conditions. Soot conversion as a function of reaction temperature over the as-prepared catalysts is profiled in Figure 1a, and the corresponding T_{50} data are listed in Table 1. All the catalysts exhibit a high CO_2 selectivity (CO_2/CO_x > 99%). The T_{50} values of CeO_2 and CuCe are 412 and 443 °C, respectively, revealing that a high Cu loading level suppresses soot oxidation over CeO_2. However, the CuCe-AE catalyst exhibits a much lower T_{50} value of 383 °C, displaying remarkably enhanced soot oxidation activity. Such a catalytic performance is normal among the Ce-based catalysts reported in the literature, as compared in Table 2, in which some important reaction parameters are also listed.

To further characterize the intrinsic activities of the as-prepared catalysts, the isothermal reactions were performed under tight contact conditions at 310 °C. At a low conversion rate (<15%), soot oxidation can be considered a surface reaction, while soot oxidation at a high conversion rate is limited by diffusion. Figure 1b shows the soot conversion amount as a function of reaction time. The reaction rate can be obtained from the slope of the lines after linear fitting, and the results are listed in Table 1. Similar to the soot–TPO results, a high Cu loading level can inhibit the reaction rate of CeO_2. After the CuCe was subjected to acid etching, the reaction rate increased from 16.2 to 46.0 μmol min^{-1} g^{-1}, which exceeds that of bare CeO_2. These data confirm that the acid etching prompts the intrinsic

reactivity of the CuO-doped CeO_2 catalyst. The E_a of catalysts was also calculated using the Arrhenius method. The Arrhenius plots of lnr vs. 1/T are shown in Figure 1c, and the corresponding parameters are listed in Table 1. The E_a of the catalysts follows a sequence of CuCe-AE (83 kJ/mol) < CeO_2 (96 kJ/mol) < CuCe (110 kJ/mol), which is in accordance with the catalytic performance in Figure 1a,b. Nevertheless, the E_a differences are not large, indicating that they conform with an identical soot oxidation reaction mechanism. To determine the stability of CuCe-AE, four consecutive cycles under the same conditions were conducted, with the results shown in Figure 1d. An obvious increase of 18 °C in the T_{50} value is observed for the second cycle, which is believed to be related importantly to the decrease in the surface area and sintering of the oxides in the used catalyst. There is no significant deactivation after the third cycle, although a small increase in the T_{50} (approximately 1–4 °C) occurs, and the catalytic behavior of the cycled CuCe-AE catalyst is still better than those of the fresh CeO_2 and CuCe. These observations indicate the potential reusability of CuCe-AE catalyst in soot combustion.

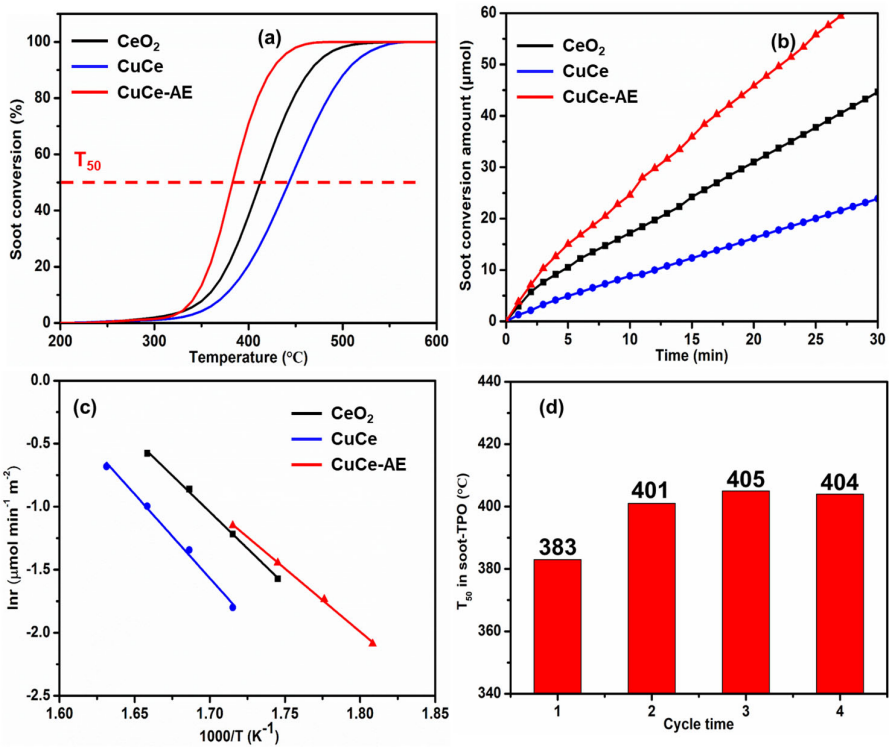

Figure 1. (**a**) Temperature−programmed oxidation of soot, (**b**) isothermal oxidation of soot at 310 °C, (**c**) Arrhenius plots of the catalysts under tight contact modes, and (**d**) cycled test of CuCe−AE catalyst.

Table 1. Reaction parameters of the catalysts for soot oxidation.

Catalyst	T_{50} (°C) [a]	S_{CO2} (%) [a]	Reaction Rate (μmol min^{-1} g^{-1}) [b]	*Ea* (kJ/mol) [c]
CeO_2	412	99.8	30.8	96
CuCe	443	99.0	16.2	110
CuCe-AE	383	99.5	46.0	83

[a] Obtained from soot-TPO. [b] Determined by isothermal reaction at 310 °C. [c] Determined by Arrhenius equation.

2.2. Physicochemical Characterization of Catalyst

Table 3 summarizes the structural and textural features of the catalysts. As determined by ICP-AES, the Cu content is 20.0 and 2.3 wt.% for CuCe and CuCe-AE, respectively. Obviously, the acid etching significantly reduces the Cu content in the CuO-doped mixed oxides.

The TEM images were collected to observe the morphologies of the catalysts. As shown in Figure 2, CeO_2 prepared by alkaline hydrothermal method displays a typical nanorod-like morphology (Figure 2a). Upon the addition of $Cu(NO_3)_2$, the CuCe (Figure 2b)

and especially CuCe-AE (Figure 2c) exhibit irregular shape. Aggregated CuO particles with a size larger than 15 nm can be clearly observed on CuCe. Figure 2d illustrates the XRD pattern of the as-prepared catalysts. The diffraction peaks at 2θ of 28.5°, 33.1°, 47.5°, 56.3°, 59.1°, 69.4°, 76.7° and 79.1° are indexed to the (111), (200), (220), (311), (222), (400), (331) and (420) planes of CeO_2 (JCPDS 34-0394). The half widths of the diffraction peak for CuO-doped catalysts are broader than pure CeO_2, indicative of a decrease in the crystallite size of the oxides. The crystallite sizes of the catalysts were calculated via the Scherrer equation, and the results are listed in Table 3. The crystallite sizes of CeO_2, CuCe and CuCe-AE are 10.5, 5.8 and 5.5 nm, respectively. In addition, the typical diffraction peaks of CuO particles appear at 2θ of 35.6 and 38.7° for the CuCe catalyst [19], suggesting the agglomeration of CuO at a high doping level. However, the diffraction peaks of CuO are not identified for CuCe-AE, implying that acid etching can remove the agglomerated CuO particles, while the highly dispersed CuO_x clusters with a size below the XRD detection limit still exist.

Table 2. Comparison of activity of CuCe-AE with Ce-based catalysts previously reported in the literature under tight contact conditions.

Catalyst	Reactant Gas	Flow Rate (mL/min)	T_{50} (°C)	Reference
CuCe-AE	$10\%O_2/N_2$	80	383	This work
$Sn_{0.7}Ce_{0.3}O_2$	O_2/N_2	268	437	3
Ru/CeO_2	$10\%O_2/N_2$	80	386	4
Cu-Ce	$10\%O_2/N_2$	500	356	13
CuO/Ce-DDA	Air	-	413	14
$Ce_{0.95}Cu_{0.05}O_2$	$10\%O_2/N_2$	100	384	19
$Cu_{0.1}Ce_{0.9}O_2$-NF	$5\%O_2/Ar$	50	310	20

Table 3. Structural and textural properties of the catalysts.

Catalyst	Cu Content (wt.%) [a]	D (nm) [b]	S_{BET} (m^2/g) [c]	V_{pore} (cm^3/g) [c]	I_D/I_{F2g} [d]
CeO_2	/	10.5	104	0.30	0.32
CuCe	20.0	5.8	98	0.22	0.38
CuCe-AE	2.3	5.4	145	0.27	0.40

[a] Determined by ICP-AES. [b] Crystallite size estimated via the Scherrer equation using the (111) peak of CeO_2. [c] Determined by N_2 sorption. [d] Obtained from Raman spectra.

To further identify Cu distribution on the catalyst surface, EDS-mapping analyses of the mixed oxides before and after acid etching were carried out, and the received images are compiled in Figure 3. The markedly agglomerated CuO particles are observed on CuCe, consistent with the XRD results. In these Cu-rich regions, a lower concentration of cerium occurs, indicating the non-uniform distribution of metal oxides. For CuCe-AE, the highly even Cu distribution is consistent with that of Ce, implying the removal of aggregated CuO particles and the reservation of homogeneously distributed mixed oxides.

The N_2 sorption isotherms and BJH pore size distribution of the catalysts are shown in Figure 4, and the BET specific surface area and pore volume results are given in Table 3. The N_2 sorption isotherms of all the catalysts show a type IV isotherm with H3 hysteresis loop, which is mainly caused by the irregular pores generated via particle accumulation. The measured pore volume is predominantly generated by the gap of primary particles. Notably, the specific surface area of CuCe-AE is about 40 m^2/g higher than that of CuCe, suggesting that acid etching can enlarge the specific surface area of CuO-doped CeO_2. A similar phenomenon was also observed by Zhao and co-workers [21]. They found that the acid-etching method not only maintained the perovskite-type structure of the $LaMnO_{3+\delta}$ catalyst, but also improved its surface area. It is generally accepted that a large specific area facilitates the contact between the soot and catalyst, being therefore beneficial for soot oxidation [23].

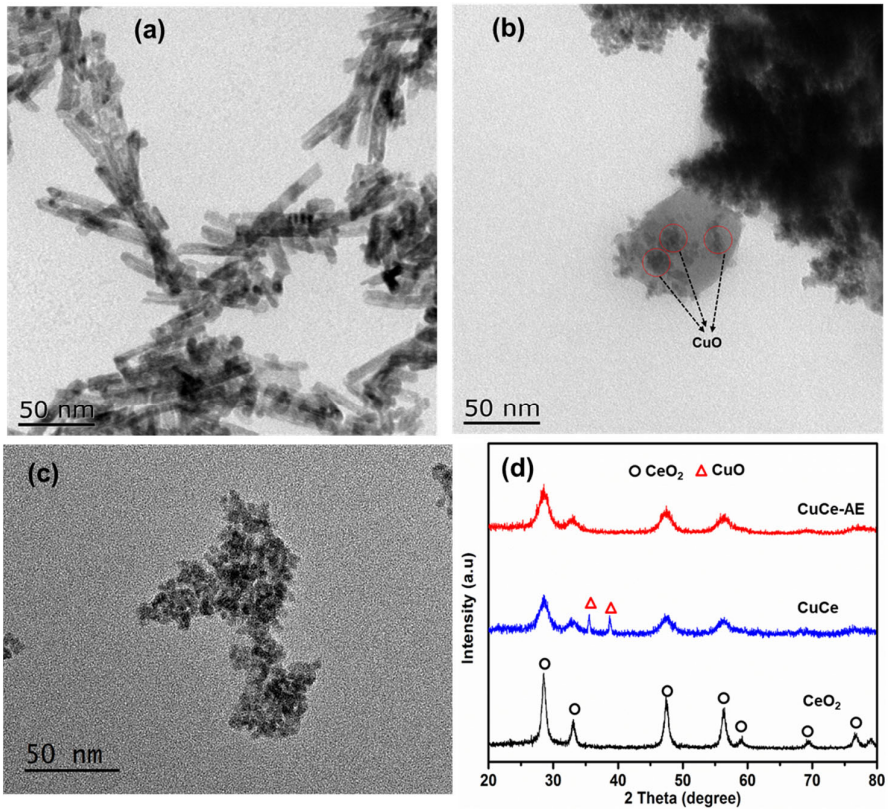

Figure 2. TEM images of (**a**) CeO_2, (**b**) CuCe and (**c**) CuCe-AE, and (**d**) XRD patterns of the catalysts.

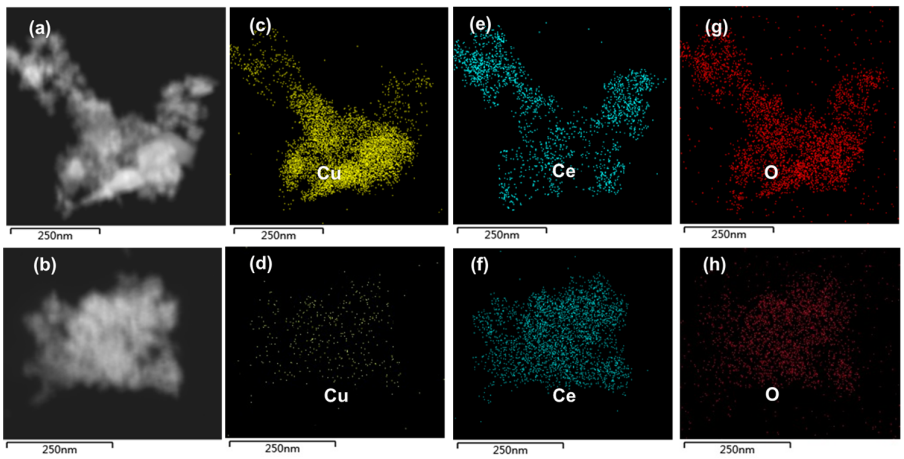

Figure 3. HAADF-STEM images of (**a**) CuCe and (**b**) CuCe-AE, and corresponding EDS elemental mapping of (**c**,**d**) Cu, (**e**,**f**) Ce, and (**g**,**h**) O.

XPS analysis was used to disclose the chemical state of Ce, O, and Cu on the catalyst surface. As listed in Table 4, the atom ratios of Cu/Ce on the surface of CuCe and CuCe-AE catalysts are 0.95 and 0.31, respectively. The measured values are not only determined by the actual content of surface elements, but also affected by the dispersion of metal oxides. Figure 5 shows the XPS full spectra of the catalysts and the fine spectrum in the Ce 3d, O 1s and Cu 2p regions, and the deconvolution results are listed in Table 4. In the spectra of Ce 3d in Figure 5b, six peaks assigned to Ce^{4+} 3d ($u_{1–6}$: 882.4, 888.6, 898.3, 900.8, 907.5, and 916.7 eV) and two peaks attributed to Ce^{3+} 3d ($v_{1–2}$: 884.5 and 902.0 eV) are observed after deconvolution [24,25]. The ratio of Ce^{3+}/Ce^{4+} decreases after CuO doping. This is due to the fact that the electronegativity of Cu (1.90) is stronger than that of Ce (1.12). After copper doping, electrons transfer from Ce to Cu ($Cu^{2+} + Ce^{3+} \rightarrow Cu^{+} + Ce^{4+}$), resulting in a

decrease in the ratio of Ce^{3+}/Ce^{4+}. A similar phenomenon was observed by Piumetti and co-workers [19]. It is generally accepted that surface oxygen vacancy is normally correlated to the content of Ce^{3+} [26]. The ratios of Ce^{3+}/Ce^{4+} for CuCe and CuCe-AE catalysts are 19.9% and 23.8%, respectively, suggesting that acid etching could increase the amount of surface oxygen vacancy on the CuO-doped CeO_2. The increased Ce^{3+}/Ce^{4+} ratio for CuCe-AE leads to an expansion of the ceria crystal cell compared with CuCe.

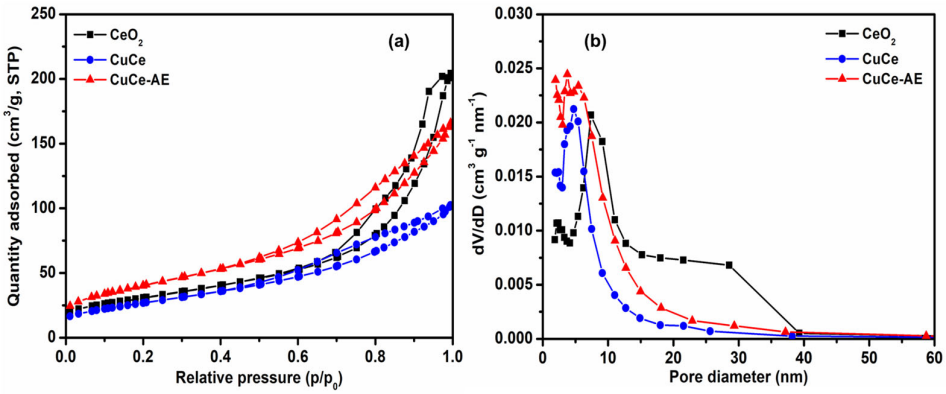

Figure 4. (**a**) N_2 adsorption−desorption isothermals and (**b**) BJH pore diameter distribution of the catalysts.

Table 4. XPS results of the catalysts.

Catalyst	Surface Cu/Ce	Ce 3d		Ce^{3+}/Ce^{4+} (%)	O 1s		O_α/O_β (%)
		Ce^{3+} (%)	Ce^{4+} (%)		O_α (%)	O_β (%)	
CeO_2	-	18.3	81.7	22.4	28	72	38.8
CuCe	0.95	16.6	83.4	19.9	25	75	33.3
CuCe-AE	0.31	19.2	80.8	23.8	38	62	61.3

Figure 5c shows the Cu 2p spectra of CuCe and CuCe-AE. The two main peaks of CuCe at the binding energies of 953 and 933 eV correspond to Cu $2p_{1/2}$ orbital and Cu $2p_{3/2}$ orbital, respectively, accompanied with two satellite peaks at the binding energies of 942 and 962 eV [27]. This result is similar to the spectrum of CuO [28], which indicates that Cu species mainly exist in the form of CuO. The CuCe-AE catalyst demonstrates weak signals in the Cu 2p region, meaning that the surface Cu content is relatively low.

Two oxygen species can be observed in the O 1s spectra in Figure 5d. The binding energy of 529–530 eV is characteristic of lattice oxygen (denoted as O_β), and the binding energy in the 531–532 eV region is related to surface oxygen species (including -OH, O_2^- and O_2^{2-}, denoted as O_α) [29,30]. The relative content of surface oxygen species can be roughly estimated by the ratio of O_α/O_β. The CuO doping results in a decrease in the proportion of O_α/O_β. This is because a great quantity of agglomerated CuO particles on the surface of CeO_2 leads to the surface oxygen species being covered. Notably, acid etching removes these aggregated CuO particles and recovers surface oxygen species to a great extent within the amount of CuO-doped CeO_2.

Raman spectroscopy of CeO_2 and CuO-doped catalysts was carried out to estimate the relative concentration of oxygen vacancies in CeO_2 lattice with an indicative at the wavelength of 532 nm [31]. As displayed in Figure 6a, the as-prepared catalysts exhibit a strong peak at ~456 cm^{-1} and two weak peaks at ~600 and 1175 cm^{-1}, which can be attributed to the F_{2g}, defect-induced (D), and second-order longitudinal optical (2LO) modes of the fluorite phase, respectively [32,33]. The ratios of I_D/I_{F2g}, as a characteristic of bulk oxygen vacancy concentration, are listed in Table 3. In comparison with pure CeO_2, CuO-doped CeO_2 shows a higher I_D/I_{F2g} ratio. The enhanced ratio of bulk oxygen vacancy in CuO-doped CeO_2 can be ascribed to the incorporation of smaller copper ions into the CeO_2 lattice ($r_{Cu}{}^{x+} < r_{Ce}{}^{x+}$). As a result, CuO doping could promote the formation of bulk

oxygen vacancy in CeO_2. The I_D/I_{F2g} ratios of CeO_2, CuCe and CuCe-AE are 0.32, 0.38 and 0.40, respectively. The CuO doping increases the bulk oxygen vacancy concentration in the mixed oxides due to distortion of the ceria crystal cell, and the acid etching creates more bulk oxygen vacancies by removing aggregated CuO particles and strengthening the interaction of highly dispersed CuO_x clusters with ceria. As we know, surface oxygen vacancy is essential for soot oxidation reaction [34]; the conclusion that enhanced bulk oxygen vacancy leads to the boosted catalytic activity may be not strict. However, the increase in bulk oxygen vacancy can accelerate the utilization of lattice oxygen CeO_2, which is responsible for improved soot oxidation activity of CuCe-AE. When the surface active oxygen is consumed by the soot, the lattice oxygen will diffuse from the bulk of the oxides onto the surface, which is closely associated with the bulk oxygen vacancy [4,35].

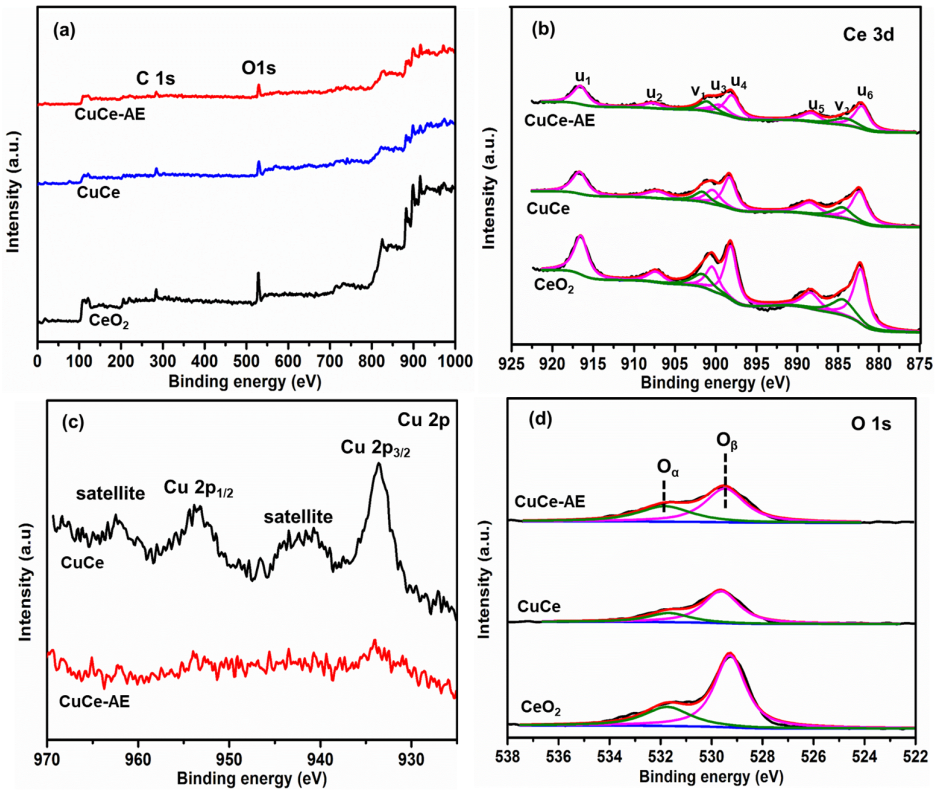

Figure 5. (**a**) The full XPS spectra of the catalysts and fine spectra of (**b**) Ce 3d, (**c**) Cu 2p, and (**d**) O 1 s.

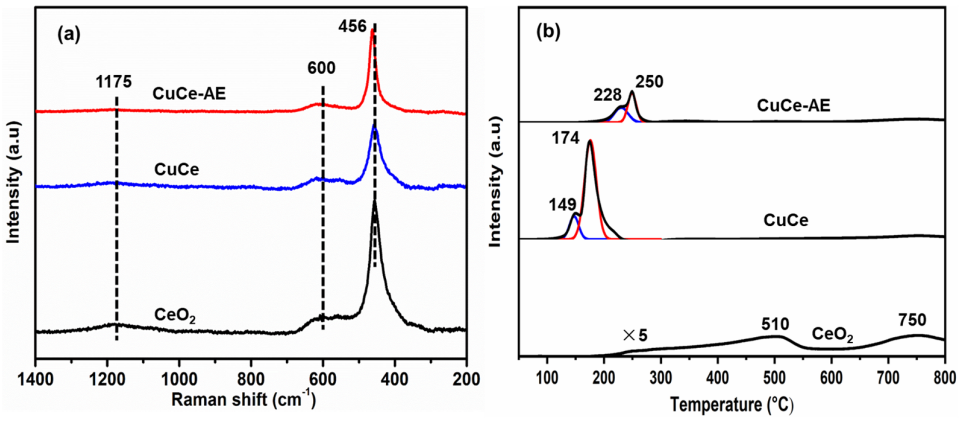

Figure 6. (**a**) Raman spectra and (**b**) H_2−TPR profiles of the catalysts.

The reducibility of the catalysts was investigated using H_2-TPR experiments, and the results are shown in Figure 6b. For pure CeO_2, two reduction peaks are observed at 510 and 750 °C, corresponding to the reduction of surface oxygen and bulk oxygen of CeO_2, respectively [36]. Two intense reduction peaks are observed at 100–200 °C for CuO-doped CeO_2, which is attributed to the reduction of CuO [37] and the promoted reduction of CeO_2 by spillover effect. The presence of multiple peaks implies the existence of different copper species with varied strength with CeO_2. The reduction peak at a low temperature (peak I) corresponds to the reduction of finely dispersed CuO_x clusters with strong interaction with CeO_2 [38,39]. The reduction peak at a high temperature (peak II) is attributed to the reduction of aggregated CuO particles with interaction with CeO_2 [39]. For the CuCe catalyst, an intense reduction peak of CuO interacting with CeO_2 at 174 °C can be clearly observed, which means that the substantial agglomerated CuO particles exist on its surface. Upon acid etching, the reduction peaks shift towards higher temperatures, and the content of aggregated CuO particles obviously decreases in peak intensity. The Gaussian fitting of the H_2-TPR curves was further conducted for CuO-doped catalysts. The area of peak I of CuCe-AE (7920) is almost identical to that of CuCe (8310), while the area of peak II decreases sharply from 44,800 to 8280 after acid etching. These results demonstrate that the acid etching almost does not affect the finely dispersed CuO_x, but removes the aggregated CuO particles significantly.

3. Experimental

3.1. Catalyst Preparation

CuCe mixed oxide catalyst with a Cu/Ce mole ratio of 1:1 was prepared using a hydrothermal method. Briefly, $Ce(NO_3)_3{\cdot}6H_2O$ (>99.9%, Nanjing Chemical Reagent, Nanjing, China) and $Cu(NO_3)_3{\cdot}3H_2O$ (>99%, Nanjing Chemical Regent) were added into deionized water. NaOH solution (>98%, Nanjing Chemical Regent) was dropped into the mixed solution slowly and magnetically stirred for 30 min. The pure CeO_2 was synthesized by a similar process but without $Cu(NO_3)_3{\cdot}3H_2O$ addition. The mixed solution was transferred into a Teflon-lined stainless-steel autoclave, which was subsequently heated at 100 °C for 24 h. After cooling to room temperature, the obtained material was washed with deionized water and alcohol for three times and dried at 80 °C overnight. Finally, the powders were calcined at 500 °C in a muffle oven for 2 h.

The CuCe sample was then washed with nitric acid to reduce the Cu content. Briefly, 1 g of CuCe was dispersed in 2 M HNO_3 solution and magnetically stirred for 12 h at room temperature. The mixture was filtered and washed with deionized water repeatedly until the filtrate was neutral. Then, the sample was dried at 80 °C in the oven overnight, and the obtained catalyst was denoted CuCe-AE.

3.2. Catalytic Activity Evaluation

Printex-U soot, which was consistently used as the model soot, was purchased from Degussa Company (Germany). In activity tests, the catalyst (50 mg) and soot (5 mg) were ground in a mortar for 5 min to achieve tight contact conditions. Tight contact maximizes the number of contact points between catalyst and soot, allows a rapid screening of catalysts, and facilitates the study of structure–performance relationships, although it is less representative of the real contact conditions that occur in a catalytic trap for diesel particulate removal [40]. To minimize the effect of hot spots caused by the exothermal nature of the reaction, the soot–catalyst mixture was diluted with silica pellets (150 mg), sandwiched by quartz wool, and placed in the vertical quartz reactor. Before each test, the mixture was pretreated in N_2 (50 mL/min) at 200 °C for 30 min to eliminate surface adsorbed species. A gas mixture of 10% O_2/N_2 (80 mL/min) was then introduced, and the mixture was heated at a ramping rate (5 °C/min) to 600 °C. The concentrations of CO_x (CO_2 and CO) in the outlet gas were measured using an infrared spectrometer (Thermo Nicolet iS10) [3,20,24]. The soot combustion efficiency was evaluated in terms of T_{50}, corresponding

to the temperature at which 50% of soot conversion was obtained. The selectivity to CO_2 was calculated using the following equation.

$$S_{CO_2}\ (\%) = A_{CO_2}/(A_{CO_2} + A_{CO}) \times 100\% \quad (1)$$

A_{CO_2} and A_{CO} represent the total peak areas of produced CO_2 and CO, respectively.

To determine the apparent activation energy (E_a) of the catalysts, the isothermal reactions were conducted under tight contact with the 10% O_2/N_2 flow of 150 mL/min. The soot conversion was kept below 15% to ensure the reaction in the kinetic regime, and the apparent activation energy was calculated according to the Arrhenius equation.

$$\ln r = A - \frac{E_a}{R} \cdot \frac{1}{T} \quad (2)$$

where A is the pre-exponential factor, R is the ideal gas constant, r is the specific soot oxidation rate (mol min^{-1} m^{-2}), and T is temperature (K).

3.3. Catalyst Characterization

The Cu content of catalysts was determined via inductively coupled plasma atomic emission spectrometry (ICP-AES, J-A1100, Jarrell-Ash, Waltham, MA, USA). The micromorphology of catalysts was characterized using a transmission electron microscope (TEM) (JEM-2100, JEOL, Tokyo, Japan). X-ray diffraction (XRD) spectra of samples were identified with an Ultima (Rigaku, Tokyo, Japan) machine operated at 40 kV and 40 mA, with a monochromator using Cu Kα radiation (λ = 0.15406 nm). The XRD diffractograms were collected in the 2θ range between 10° and 80°, with a step size of 10°/min. To check the distribution of Cu element in samples, an energy-dispersive spectrometry (EDS) analysis was carried out. The specific surface area of catalysts was measured via N_2 sorption at −196 °C using the Brunauer–Emmett–Teller (BET) method on an ASAP 2020 apparatus (Micromeritics, Unterschleissheim, Germany). The sample was vacuum-pretreated at 300 °C for 3 h prior to measurement. The H_2 temperature-programmed reduction (H_2-TPR) was carried out on a Finesorb-3010 instrument (Fantai, Hangzhou, China) equipped with a thermal conductivity detector (TCD). About 10 mg of the sample was placed in a U-shaped quartz tube and pretreated in N_2 (50 mL/min) at 200 °C for 1 h. After cooling to room temperature, 7.0 vol% H_2/Ar (50 mL/min) was introduced, and the sample was then heated from 25 to 800 °C with a ramp rate of 10 °C/min. Raman spectroscopy of samples was performed on a LabRAM Aramis (Horiba, Tokyo, Japan) with a 532 nm Ar^+ laser beam. The valence states of surface O, Ce and Cu were acquired via X-ray photoelectron spectroscopy (XPS) (ULVAC-PHI5000, Kanagawa, Japan). The binding energy was calibrated with a C1s peak at 284.6 eV.

4. Conclusions

In this work, acid etching was applied to tune the loading amount and form of copper oxide species in ceria-based mixed oxides. An abnormal decrease in the soot oxidation activity of a CuO-doped CeO_2 catalyst was observed, with a T_{50} increase of 31 °C. This was ascribed to the extra high Cu loading (20 wt.%), resulting in the formation of aggregated CuO particles in addition to highly dispersed CuO_x clusters. The strong interaction of CuO_x clusters with CeO_2 promoted the formation of bulk oxygen vacancy in CeO_2, but the amount of surface oxygen species decreased obviously due to coverage by agglomerated CuO particles. Correspondingly, the intrinsic reactivity of CuCe was reduced for soot oxidation.

Importantly, these aggregated CuO particles can be removed via acid etching, resulting in a remarkable increase in the catalyst surface area and restoration of surface oxygen vacancies. Meanwhile, highly dispersed CuO_x clusters facilitating the generation of bulk oxygen vacancy are mostly reserved in the etched catalyst. As a result, the etched mixed

oxides show the lowest light-off temperature and apparent activation energy for soot oxidation via an enhanced Mv-K reaction mechanism.

Author Contributions: Conceptualization, C.Z. and X.W.; Data curation, C.Z. and X.W.; Formal analysis, C.Z. and Z.L.; Funding acquisition, X.W. and D.W.; Investigation, C.Z. and X.W.; Methodology, R.R. and X.W.; Project administration, D.W.; Resources, Z.L., R.R. and D.W.; Supervision, X.W.; Visualization, Z.L. and R.R.; Validation, Z.L.; Writing—original draft, C.Z.; Writing—review and editing, C.Z., X.W., Z.L. and R.R. All authors have read and agreed to the published version of the manuscript.

Funding: This work was financially supported by projects of the National Key Research and Development Program of China (No. 2023YFC3707202), Mobile Source Emission Control Technology (NELMS2020A08) and Key Laboratory of Advanced Materials of Ministry of Education of China (ADV22-18).

Data Availability Statement: Data are contained within the article.

Acknowledgments: The authors would like to thank the help from Letong Yang and Letao Li.

Conflicts of Interest: The authors declare that they have no known competing financial interest or personal relationships that could have appeared to influence the work that was reported in this paper.

References

1. Li, Y.; Guo, H.; Xiong, J.; Ma, Y.; Li, X.; Zhang, P.; Zhang, S.; Wei, Y. The Catalyst of Ruthenium Nanoparticles Decorated Silicalite-1 Zeolite for Boosting Catalytic Soot Oxidation. *Catalysts* **2022**, *13*, 1167. [CrossRef]
2. Leonardi, S.A.; Miró, E.E.; Milt, V.G. Activity of catalytic ceramic papers to remove soot particles-A study of different types of Soot. *Catalysts* **2022**, *12*, 855. [CrossRef]
3. Zhu, S.; Shi, S.; Zheng, X.; Wang, X.; Yu, G.; Jiang, Y.; Feng, J.; Zhu, L.; Zhang, G. Enhanced oxygen vacancies in Ce-Doped SnO_2 nanofibers for highly efficient soot catalytic combustion. *Catalysts* **2022**, *12*, 596. [CrossRef]
4. Zheng, C.; Mao, D.; Xu, Z.; Zheng, S. Strong Ru-CeO_2 interaction boosts catalytic activity and stability of Ru supported on CeO_2 nanocube for soot oxidation. *J. Catal.* **2022**, *411*, 122–134. [CrossRef]
5. Zhang, H.; Hu, W.; Zhou, C.; Liu, H.; Yao, P.; Wang, J.; Chen, Y. A new understanding of CeO_2-ZrO_2 catalysts calcinated at different temperatures: Reduction property and soot-O_2 reaction. *Appl. Catal. A* **2018**, *563*, 204–215. [CrossRef]
6. Ji, F.; Men, Y.; Wang, J.; Sun, Y.; Wang, Z.; Zhao, B.; Tao, X.; Xu, G. Promoting diesel soot combustion efficiency by tailoring the shapes and crystal facets of nanoscale Mn_3O_4. *Appl. Catal. B* **2019**, *242*, 227–237. [CrossRef]
7. Xu, J.; Lu, G.; Guo, Y.; Guo, Y.; Gong, X. A highly effective catalyst of Co-CeO_2 for the oxidation of diesel soot: The excellent NO oxidation activity and NO_x storage capacity. *Appl. Catal. A* **2017**, *535*, 1–8. [CrossRef]
8. Zhang, Z.; Han, D.; Wei, S.; Zhang, Y. Determination of active site densities and mechanisms for soot combustion with O_2 on Fe-doped CeO_2 mixed oxides. *J. Catal.* **2010**, *276*, 16–23. [CrossRef]
9. Lin, X.; Li, S.; He, H.; Wu, Z.; Wu, J.; Chen, L.; Ye, D.; Fu, M. Evolution of oxygen vacancies in MnO_x-CeO_2 mixed oxides for soot oxidation. *Appl. Catal. B* **2018**, *223*, 91–102. [CrossRef]
10. Zhang, H.; Zhou, C.; Galvez, M.; Costa, P.; Chen, Y. MnO*x*-CeO_2 mixed oxides as the catalyst for NO-assisted soot oxidation: The key role of NO adsorption/desorption on catalytic activity. *Appl. Surf. Sci.* **2018**, *462*, 678–684. [CrossRef]
11. Jia, A.; Jiang, S.; Lu, J.; Luo, M. Study of catalytic activity at the CuO-CeO_2 interface for CO oxidation. *J. Phys. Chem. C* **2010**, *114*, 21605–21610. [CrossRef]
12. Davó-Quinonero, A.; Navlani-García, M.; Lozano-Castelló, D.; Bueno-López, A.; Anderson, J.A. Role of hydroxyl groups in the preferential oxidation of CO over copper oxide-cerium oxide catalysts. *ACS Catal.* **2016**, *6*, 1723–1731. [CrossRef]
13. Liang, Q.; Wu, X.; Weng, D.; Xu, H. Oxygen activation on Cu/Mn–Ce mixed oxides and the role in diesel soot oxidation. *Catal. Today* **2008**, *139*, 113–118. [CrossRef]
14. Nakagawa, K.; Ohshima, T.; Tezuka, Y.; Katayama, M.; Katoh, M.; Sugiyama, S. Morphological effects of CeO_2 nanostructures for catalytic soot combustion of CuO/CeO_2. *Catal. Today* **2015**, *246*, 67–71. [CrossRef]
15. Avgouropoulos, G.; Ioannides, T. Selective CO oxidation over CuO-CeO_2 catalysts prepared via the urea–nitrate combustion method. *Appl. Catal. A* **2003**, *244*, 155–167. [CrossRef]
16. Heynderickx, P.M.; Thybaut, J.W.; Poelman, H.; Poelman, D.; Marin, G.B. The total oxidation of propane over supported Cu and Ce oxides: A comparison of single and binary metal oxides. *J. Catal.* **2010**, *272*, 109–120. [CrossRef]
17. Wang, J.; Cheng, L.; An, W.; Xu, J.; Men, Y. Boosting soot combustion efficiencies over CuO–CeO_2 catalysts with a 3DOM structure. *Catal. Sci. Technol.* **2016**, *6*, 7342–7350. [CrossRef]
18. Andana, T.; Piumetti, M.; Bensaid, S.; Veyre, L.; Thieuleux, C.; Russo, N.; Fino, D.; Quadrelli, E.A.; Pirone, R. CuO nanoparticles supported by ceria for NO_x-assisted soot oxidation: Insight into catalytic activity and sintering. *Appl. Catal. B* **2017**, *216*, 41–58. [CrossRef]

19. Piumetti, M.; Bensaid, S.; Andana, T.; Russo, N.; Pirone, R.; Fino, D. Cerium-copper oxides prepared by solution combustion synthesis for total oxidation reactions: From powder catalysts to structured reactors. *Appl. Catal. B* **2017**, *205*, 455–468. [CrossRef]
20. Cui, B.; Yan, S.; Xia, Y.; Li, K.; Li, S.; Wang, D.; Ye, Y.; Liu, Y. $Cu_xCe_{1-x}O_2$ nanoflakes with improved catalytic activity and thermal stability for diesel soot combustion. *Appl. Catal. A* **2019**, *578*, 20–29. [CrossRef]
21. Zhao, B.; Ran, R.; Sun, L.; Guo, X.; Wu, X.; Weng, D. NO catalytic oxidation over an ultra-large surface area $LaMnO_{3+\delta}$ perovskite synthesized by an acid-etching method. *RSC Adv.* **2016**, *6*, 69855–69860. [CrossRef]
22. Liang, F.; Yu, Y.; Zhou, W.; Xu, X.; Zhu, Z. Highly defective CeO_2 as a promoter for efficient and stable water oxidation. *J. Mater. Chem. A* **2015**, *3*, 634–640. [CrossRef]
23. Wei, Y.; Liu, J.; Zhao, Z.; Duan, A.; Jiang, G.; Xu, C.; Gao, J.; He, H.; Wang, X. Three-dimensionally ordered macroporous $Ce_{0.8}Zr_{0.2}O_2$-supported gold nanoparticles: Synthesis with controllable size and super-catalytic performance for soot oxidation. *Energy Environ. Sci.* **2011**, *4*, 2959–2970. [CrossRef]
24. Ji, J.; Jing, M.; Wang, X.; Tan, W.; Guo, K.; Li, L.; Wang, X.; Song, W.; Cheng, L.; Sun, J.; et al. Activating low-temperature NH_3-SCR catalyst by breaking the strong interface between acid and redox sites: A case of model $Ce_2(SO_4)_3$-CeO_2 study. *J. Catal.* **2021**, *399*, 212–223. [CrossRef]
25. Li, J.; Liu, Z.; Cullen, D.; Hu, W.; Huang, J.; Yao, L.; Peng, Z.; Liao, P.; Wang, R. Distribution and valence state of Ru species on CeO_2 supports: Support shape effect and its influence on CO oxidation. *ACS Catal.* **2019**, *9*, 11088–11103. [CrossRef]
26. Deng, X.; Li, M.; Zhang, J.; Hu, X.; Zheng, J.; Zhang, N.; Chen, B. Constructing nano-structure on silver/ceria-zirconia towards highly active and stable catalyst for soot oxidation. *Chem. Eng. J.* **2017**, *313*, 544–555. [CrossRef]
27. Zhang, C.; Wang, J.; Yang, S.; Liang, H.; Men, Y. Boosting total oxidation of acetone over spinel MCo_2O_4 (M = Co, Ni, Cu) hollow mesoporous spheres by cation-substituting effect. *J. Colloid Interface Sci.* **2019**, *539*, 65–75. [CrossRef] [PubMed]
28. Yang, S.; Wang, J.; Chai, W.; Zhu, J.; Men, Y. Enhanced soot oxidation activity over CuO/CeO_2 mesoporous nanosheets. *Catal. Sci. Technol.* **2019**, *9*, 1699–1709. [CrossRef]
29. Othmane, A.; Essamlali, Y.; Fihri, A.; Larzek, M.; Zahouily, M. Effect of calcination temperature on the structure and catalytic performance of copper-ceria mixed oxide catalysts in phenol hydroxylation. *RSC Adv.* **2017**, *7*, 12586–12597.
30. Xu, X.; Liu, L.; Tong, Y.; Fang, X.; Xu, J.; Jiang, D.; Wang, X. Facile Cr^{3+}-doping strategy dramatically promoting Ru/CeO_2 for low-temperature CO_2 methanation: Unraveling the roles of surface oxygen vacancies and hydroxyl groups. *ACS Catal.* **2021**, *11*, 5762–5775. [CrossRef]
31. Chang, S.; Li, M.; Hua, Q.; Zhang, L.; Ma, Y.; Ye, B.; Huang, W. Shape-dependent interplay between oxygen vacancies and Ag–CeO_2 interaction in Ag/CeO_2 catalysts and their influence on the catalytic activity. *J. Catal.* **2012**, *293*, 195–204. [CrossRef]
32. Wu, Z.; Li, M.; Howe, J.; Meyer, H.M.; Overbury, S.H. Probing defect sites on CeO_2 nanocrystals with well-defined surface planes by Raman spectroscopy and O_2 adsorption. *Langmuir* **2010**, *26*, 6595–16606. [CrossRef] [PubMed]
33. Li, Y.; Wei, Z.; Gao, F.; Kovarik, L.; Peden, C.H.F.; Wang, Y. Effects of CeO_2 support facets on VO_x/CeO_2 catalysts in oxidative dehydrogenation of methanol. *J. Catal.* **2014**, *315*, 15–24. [CrossRef]
34. Mao, X.; Liu, S.; Liu, W.; Wu, X.; Liu, S. A simple model catalyst study to distinguish the roles of different oxygen species in propane and soot combustion. *Appl. Catal. B* **2022**, *310*, 121331. [CrossRef]
35. Gao, Y.; Duan, A.; Liu, S.; Wu, X.; Liu, W.; Li, M.; Chen, S.; Wang, X.; Weng, D. Study of $Ag/Ce_xNd_{1-x}O_2$ nanocubes as soot oxidation catalysts for gasoline particulate filters: Balancing catalyst activity and stability by Nd doping. *Appl. Catal. B* **2017**, *203*, 116–126. [CrossRef]
36. Cárdenas-Arenas, A.; Quindimil, A.; Davó-Quiñonero, Q.; Bailón-García, E.; Lozano-Castelló, D.; De-La-Torre, U.; Pereda-Ayo, B.; González-Marcos, J.A.; González-Velasco, J.R.; Bueno-López, A. Isotopic and In Situ DRIFTS study of the CO_2 methanation mechanism using Ni/CeO_2 and Ni/Al_2O_3 catalysts. *Appl. Catal. B* **2020**, *265*, 118538. [CrossRef]
37. Zimmer, P.; Tschöpe, A.; Birringer, R. Temperature-programmed reaction spectroscopy of ceria- and Cu/ceria-supported oxide catalyst. *J. Catal.* **2002**, *205*, 339–345. [CrossRef]
38. Sun, S.; Mao, D.; Yu, J.; Yang, Z.; Lu, G.; Ma, Z. Low-temperature CO oxidation on CuO/CeO_2 catalysts: The significant effect of copper precursor and calcination temperature. *Catal. Sci. Technol.* **2015**, *5*, 3166–3181. [CrossRef]
39. Gamarra, D.; Cámara, A.L.; Monte, M.; Rasmussen, S.B.; Chinchilla, L.E.; Hungría, A.B.; Munuera, G.; Gyorffy, N.; Schay, Z.; Corberán, V.C.; et al. Preferential oxidation of CO in excess H_2 over CuO/CeO_2 catalysts: Characterization and performance as a function of the exposed face present in the CeO_2 support. *Appl. Catal. B* **2013**, *130–131*, 224–238. [CrossRef]
40. Piumetti, M.; Bensaid, S.; Russo, N.; Fino, D. Nanostructured ceria-based catalysts for soot combustion: Investigations on the surface sensitivity. *Appl. Catal. B* **2015**, *165*, 742–751. [CrossRef]